Journal of Applied Electrochemistry **29**: 1053–1061, 1999.

Anodic dissolution of aluminium in organic electrolytes containing perfluoroalkylsulfonyl imides

L. PÉTER** and J. ARAI*
Hitachi Research Laboratory, 1-1 Omika-cho 7-chome, Hitachi-shi, Ibaraki-ken 319-12, Japan
*(*author for correspondence, e-mail: jarai@hrl.hitachi.co.jp)*
*(**Present address: Research Institute for Solid State Physics and Optics, Hungarian Academy for Sciences, H-1525 Budapest, PO Box 49, Hungary)*

Received 6 October 1998; accepted in revised form 19 January 1999

Key words: aluminium, anodic dissolution, lithium ion battery, nonaqueous electrolyte, perfluoroalkylsulfonyl imides

Abstract

Electrochemical dissolution of aluminium has been investigated in various solutions composed of organic solvents and 1 M lithium bis(perfluoroalkylsulfonyl) imide salts. Potentials of the onset of transpassive dissolution and repassivation as well as dissolution currents have been measured for several systems by using voltammetric methods. Empirical correlation between the composition of the solvent and the dissolution current has been established for mixtures of ethylene carbonate and ethylmethyl carbonate. The effect of the perfluoroalkyl chain length on the dissolution rate has also been studied and the result has been elucidated with the help of considerations on the structure of the ions. Mechanistic information obtained from electrochemical impedance spectra revealed that at least two adsorbed intermediates have to be included in the dissolution mechanism. Conditions of application of lithium perfluoroalkylsulfonyl imides in lithium ion batteries are briefly discussed.

1. Introduction

Most types of secondary lithium ion batteries are based on intercalation materials employed in both the cathode and the anode and electrolytes containing organic solvents with dissolved lithium salts. Organic carbonates are the most common solvents used in secondary lithium ion batteries due to their high kinetic stability towards oxidation and ability to produce a compact film on carbon anodes. Single solvent systems can hardly ever fulfill all requirements, therefore blends of different carbonates (and sometimes ethers) are preferred in which the properties of the individual components can be tailored and appropriate viscosity, vapour pressure, dielectric constant, solubility of lithium salts and chemical stability can be achieved. The number of salts suitable for such electrolytes is limited. The general approach is to apply a salt of the $LiXF_n$ type where $n = 4$ if X is boron and $n = 6$ if X is phosphorous or arsenic. All the members of the $LiXF_n$ family are unstable in the presence of water and produce HF which is known to lead to a capacity loss by dissolving the cathode material [1–3]. Furthermore, insufficient thermal stability is also a serious disadvantage of the $LiXF_n$ compounds. Disposal of batteries containing $LiAsF_6$ raises serious concern on environmental protection, too.

Several other classes of lithium salts have been developed in the last decade. Lithium organoborates ([4] and literature cited therein) and lithium bis(perfluoroalkylsulfonyl) imides (LiBPSIs) are the most promising candidates in commercial battery applications. LiBPSIs exhibit excellent thermal and hydrolytic stability coupled with good solubility in practically every solvent applied in lithium batteries [5, 6]. Another advantage is that the molar conductivity of the LiBPSI solutions is superior to that of the conventional $LiXF_n$ electrolytes through the whole temperature range for which lithium batteries are designed [5]. The main reason why LiBPSIs are not yet employed in commercial batteries is that aluminium, which is almost exclusively used as the current collector for cathode materials, severely corrodes in the presence of LiBPSIs [6, 7]. Though the impact of LiBPSIs on aluminium appears to be generally known, very little attention has been paid to the investigation of the reaction mechanism. The extent of the problem of aluminium dissolution was assessed by measuring the decay of the dissolution current with time and analysing the passive layer on aluminium [6]. No compatibility problem occurs with carbon anodes and copper current collectors hence lithium bis(trifluoromethylsulfonyl) imide (LiTFSI) has been used successfully for analysis of the performance of solvent blends and carbon anodes [8, 9].

The aim of present work was to study the kinetics and mechanism of the LiBPSI-induced dissolution of aluminium in solvents that are identical with or similar to those applied in commercial batteries. Ethylmethyl carbonate (EMC) and ethylene carbonate (EC) were selected to investigate the impact of a solvent of molecules with low and high dipole moment, respectively. EC is an essential component of solvent blends due to its beneficial effect on the lithium ion conducting film on carbon ([9–11] and literature cited therein). Asymmetric dialkyl carbonates like EMC are also necessary to attain good cell cyclability [11, 12]. Propylene carbonate (PC), trifluoropropylene carbonate (TFPC) and their mixtures with EC or EMC were investigated as well. 1,2-dimethoxy ethane (DME) was also employed in order to exclude any specific interaction between the carbonate-type solvent and aluminium. The effect of the perfluoroalkyl chain length in LiBPSIs was examined by using LiTFSI and lithium bis(pentafluoroethylsulfonyl) imide (LiBETI). The difference observed in the activity of LiTFSI and LiBETI towards aluminium corrosion has been elucidated with the help of data from molecular orbital calculation.

2. Experimental details

Solvents such as EMC, EC, PC and DME of battery grade with water content typically less than 20 ppm were purchased from Tomiyama Yakuhin Kogyo K.K. and used as received. TFPC was the product of Japan Energy K.K. and featured the same purity as the other solvents. Solvent molar mixing ratios are given as percentages throughout this paper. Purity of LiTFSI, LiBETI (both from 3M) and $LiPF_6$ (Hashimoto Kaisei KK) was better than 99%. All lithium salts were used after vacuum drying. Electrode specimens were made of commercial 99.5% pure aluminium. Previous results confirm that purity of aluminium beyond this level has very little impact on the pitting behaviour in the media studied [13]. Chemicals were stored in a glove box with constantly purified argon atmosphere. The due point of H_2O was maintained below $-80\,^{\circ}C$.

A single-compartment whole-Teflon cell (Hokuto Denko) of 2 cm^3 total volume was used in all experiments but bulk electrolysis. Aluminium electrodes were fitted as a screw to the bottom of the cell. Geometric surface area of the flat aluminium electrodes was 0.785 cm^2. Aluminium samples were polished with dry emery paper to a mirror finish prior to the cell assembly. The polishing process was carried out either under argon atmosphere or in the air. Electrode prehistory is indicated in the text whenever it is of importance. The lithium disc counterelectrode and lithium ring reference electrode were connected through side fittings. Potentials are referred to the rest potential of the lithium reference electrode immersed into the same solution (Li/Li^+).

Bulk electrolysis experiments were carried out in a two-compartment cell with two layers of commercial porous polyethylene separator between the compartments. This cell was operated in a two-electrode configuration with aluminium foil working electrode and lithium counter/reference electrode.

Electrochemical data were obtained by using a Hokuto Denko workstation including an HB-105 function generator, an HA-501G potentiostat–galvanostat and an NF 5080 frequency response analyzer. The workstation was controlled with an NEC computer and software provided by Hokuto Denko. Solution analysis was carried out with a Hitachi P-4000 Inductively Coupled Plasma (ICP) spectrometer by using appropriate reference solutions as external standards.

The optimized structure of the perfluoroalkylsulfonyl imide anions were calculated by using an *ab initio* molecular orbital simulation (gaussian 94W program by Gaussian, Inc.) with the unrestricted Hartree–Fock method and the basis set of 6-31G** (adding polarization effects to atomic orbitals) [14]. Bond angles from the output files are used for structural analysis.

3. Experimental results

Two methods of electrode polarization were used in this study. Potential against time function for both methods is plotted in Figure 1. Interestingly, the two methods led to distinctively different results and thus discussed separately though the reasons of this unusual behaviour is not yet understood.

3.1. *Polarization with potential sweep only*

Experiments described in this section were carried out by using method 1 as shown in Figure 1. First, the open circuit potential of the electrode was measured, then the electrode was polarized with potentiostatic condition to the open circuit potential for 5 min. After this treatment the potential was scanned at 5 mV s^{-1} sweep rate up to the anodic limit and then down to the initial potential. At least 10 subsequent cycles were carried out in most of the experiments.

3.1.1. *Experiments with electrodes polished at ambient conditions*

In the first series of experiments, electrodes polished at ambient conditions were used; therefore, the surface of the samples was covered with a native oxide layer. Depending on the solution applied, current either decreased or increased with cycle number. Typical potentiodynamic curves of both types are illustrated in Figures 2 and 3.

Curves similar to those shown in Figure 2 were obtained for a number of solution that will be referred to as noncorrosive systems and moderately corrosive systems, consistently with the classification described in Table 1. Data shown in Figure 2 do not provide any evidence of pitting corrosion or high-rate dissolution previously associated with LiTFSI but rather indicate

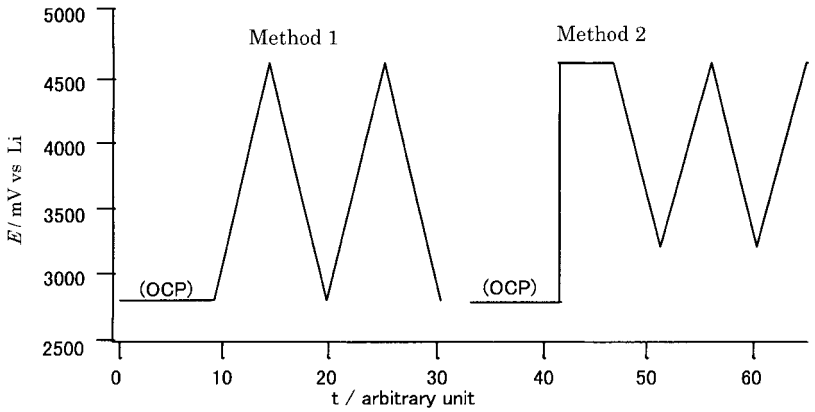

Fig. 1. Potential programs applied in potentiodynamic measurements. Method 1: initial treatment at the open circuit potential followed by sweeps of 5 mV s^{-1} (no potential step is applied). Method 2: potential step followed by sweeps of 5 mV s^{-1}.

that the electrode is passivated. Maximum current densities at 4.60 V (i.e., the anodic limit for solutions with 1 M LiTFSI) is usually about 10 μA cm^{-2} in the first cycle and decreases with cycling down to approximately 3 to 6 μA cm^{-2} in the 10th cycle. The extent of the decrease in current density is even more pronounced if $LiPF_6$ is applied as a solute, either alone or with some LiBPSI cosolute. Currents at a particular potential measured during the anodic scans always exceeds the current obtained in the subsequent cathodic sweep at the same potential. This feature of the potentiodynamic curves is consistent with the assumption that the electrode surface is covered with a passive layer which becomes thicker or more compact when the potential cycles are performed.

Amongst the solutions examined, 1 M LiTFSI/PC and 1 M LiTFSI/PC–EC (at any mixing ratio available) result in the pitting corrosion of aluminium during the experiments with potential sweep only. These systems will be labelled as very corrosive solutions. For the 1 M LiTFSI/PC solution (Figure 3), current in the first cycle achieves a maximum in the cathodic sweep with a typical current density of 40 μA cm^{-2}. Currents in the subsequent cycles are substantially higher and ultimately such dissolution conditions are attained that the loop disappears from the potentiodynamic curves and high-rate dissolution takes place from about 3.55 V. The latter data is in excellent agreement with the observation of Krause et al. [6]. Semilogarithmic plot of the polarization curve exhibits a Tafel region with a slope of 125 mV $decade^{-1}$ in the 3.6–3.8 V interval. The deviation from the Tafel line beyond 3.8 V cannot be corrected with an ohmic drop compensation and therefore it is assumed that mass transport limitations account for the lower-than-expected currents. The corrosion rate of aluminium determined with the help of the extrapolation of the Tafel line (observed between 3.6 and 3.8 V) to the rest potential (2.86 V) is 0.8 μA cm^{-2}.

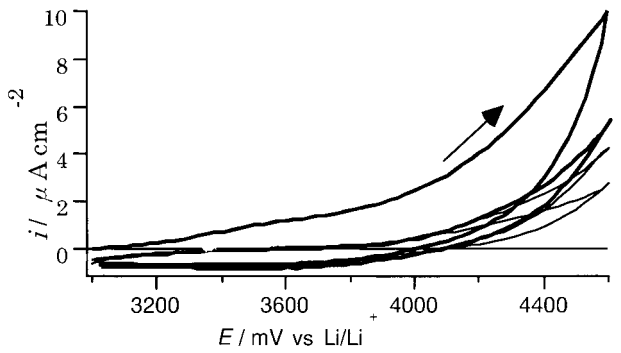

Fig. 2. Typical potentiodynamic curves obtained with method 1. Electrode, aluminium polished in air. Solution: 1 M LiTFSI/TFPC. Thick solid line: first cycle; thick broken line: second cycle; thin solid line: third cycle; thin dotted line: tenth cycle. Arrow indicates the scan direction.

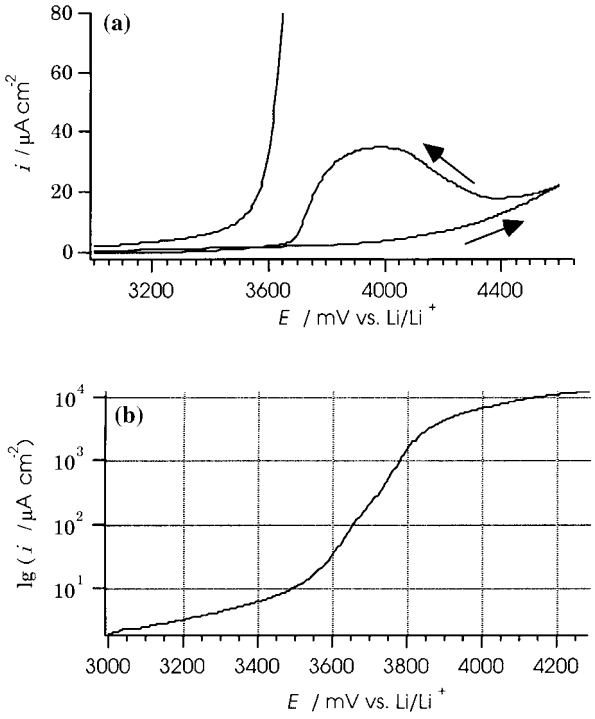

Fig. 3. Voltammetric data for 1 M LiTFSI/PC solution. Electrode, aluminium polished in air. (a) Solid line: first cycle; broken line: sweep after extensive anodic treatment. (b) semilogarithmic plot of the steady-state curve. Arrows indicate the scan direction.

Table 1. Classification of the solutions studied from the viewpoint of aluminium dissolution and passivation

	Noncorrosive systems	Moderately corrosive systems	Very corrosive systems
Solution types (with examples studied)	*Solutions with $LiPF_6$, $LiBF_4$ and/or LiF* 1 M $LiPF_6$/EMC 0.9 M $LiPF_6$ + 0.1 M LiF/EMC 1 M $LiPF_6$/PC 1 M $LiBF_4$ /PC *Solutions with some LiBPSI and $LiPF_6$ or $LiBF_4$ as a cosolute* 0.3 M LiTFSI + 0.7 M $LiPF_6$ /EMC + 30% EC	*Solvents except PC with LiTFSI and/or LiBETI* 1 M LiTFSI/EMC 1 M LiBETI/EMC 1 M LiTFSI/EMC + EC with 0–30% EC 1 M (LiFTSI/LiBETI)/EMC + 30% EC 1 M LiTFSI/TFPC 1 M LiTFSI/TFPC + 50% EMC 1 M LiTFSI/DME	*Solutions with PC and LiTFSI* 1 M LiTFSI/PC 1 M LiTFSI/PC + 50% EC
Common features	No activation of aluminium is observed	No activation of aluminium is observed with method 1 but rapid dissolution is achieved with method 2	Pitting corrosion and then rapid dissolution is observed by using any type of polarization program

3.1.2. *Experiments with electrodes polished under argon*
In the second series of experiment, the aluminium samples were polished in the glove box just before the cell was assembled. It is assumed that most of the native oxide was removed from the aluminium surface. Although the 'bare' aluminium surface is very reactive, the available reagents (for instance, solvent vapour and later the electrolyte solution) form a less compact layer than oxygen. Potentiodynamic experiments (method 1 in Figure 1) lead to the same classification as in case of oxide-covered electrodes.

The removal of the oxide layer by polishing aluminium under argon atmosphere decreases the open circuit potential of aluminium. The rest potential immediately after immersion is usually 1.4–1.8 V and increases to the rest potential determined for oxide-covered aluminium over a few hours.

In noncorrosive or moderately corrosive systems, the current for aluminium with no native oxide is 3 to 12 times higher in the first cycle than in case of oxide-covered electrodes. No electrochemical evidence of pitting corrosion was found. The current decay with cycling is similar to that measured for oxide-covered electrodes and the current at 4.6 V in the 10th cycle is often the same. Data for very corrosive systems shows more severe pitting corrosion in the first potential cycle, and the electrode development from pitting corrosion to active dissolution is much faster if the native oxide is removed.

3.2. *Polarization with potential step followed by potential sweeps*

Method 2 as shown in Figure 1 was applied in the experiments discussed below. Aluminium electrodes were polarized to a highly oxidizing potential for 1 to 5 min, then cyclic voltammograms were run by starting with the cathodic scan. Direction of the potential sweep was reversed at a potential no lower than 3.2 V.

Behaviour of aluminium is essentially the same with method 1 and method 2 in noncorrosive systems; that is, aluminium remains passive and currents at a particular potential decrease with cycling. However, the potential step in method 2 is capable of activating aluminium electrodes immersed into moderately corrosive electrolyte solutions. Activation is equally achievable for electrodes with a native oxide and for those polished under argon atmosphere, hence the two cases no longer need to distinguish. On the cathodic scan (i.e., first half-cycle) current remains high until the potential of current cut-off is reached, then drops down to the μA cm^{-2} level. On the anodic scan (second half-cycle) current slowly increases until the potential of current onset is attained and then returns to the same level as observed at the beginning of the experiment. The current onset is followed by a current maximum if the dissolution rate is higher than 2 μA cm^{-2} due to the relaxation of the diffusion field.

Results obtained for 1 M LiTFSI/EC + EMC solutions are plotted in Figure 4. The higher the molar fraction of EC in the solvent blend the higher the current in the potential interval of dissolution and the lower the potential of both the current onset and the current cut-off. Curves plotted in Figure 4 were obtained at 5 mV s^{-1} sweep rate but it was confirmed that the deviation from the results shown is insignificant if the sweep rate lies within the 1–30 mV s^{-1} interval. The effect of the decrease in the sweep rate is the depression of the current maximum which occurs after the electrode is activated during the anodic scan. The decrease in the cathodic scan reversal potential does not impact either the potential of the current onset or the current measured at high anodic potentials, as it can be seen Figure 5. The linear regions occurring in the semilogarithmic plot were used to determine the potential of the current onset and the current cut-off.

Gradual substitution of LiTFSI with LiBETI by using a particular solvent blend leads to the shift of voltammetric curves to more anodic potentials. Figure 6 illustrates that the potentials of both the current onset and current cut-off increase with the concentration of LiBETI. The dissolution rate measured at a sufficiently

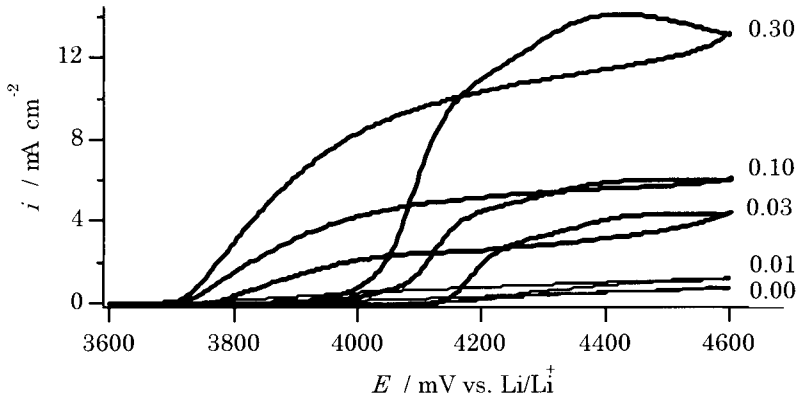

Fig. 4. Voltammetric data obtained with method 2. Solutions: 1 M LiTFSI/EMC + EC. Numbers on the right edge of the Figure denote the molar fraction of EC for each curves.

high anodic potential decreases with LiBETI concentration though this change in the current is substantially smaller than the current drop around the potential of the current cut-off. Potentials of the current onset and the current cut-off for several systems are summarized in Table 2.

Addition of $LiPF_6$ to any solution containing LiTFSI inhibits the dissolution of aluminium and the decrease in the anodic current is by orders of magnitude larger than the change in the electrolyte composition. The inhibition is detected with $LiBF_4$ as well. In these cases, the current remains low even after a step in potential and the curves obtained are similar to those measured for solutions with 1 M $LiPF_6$ but without a cosolute.

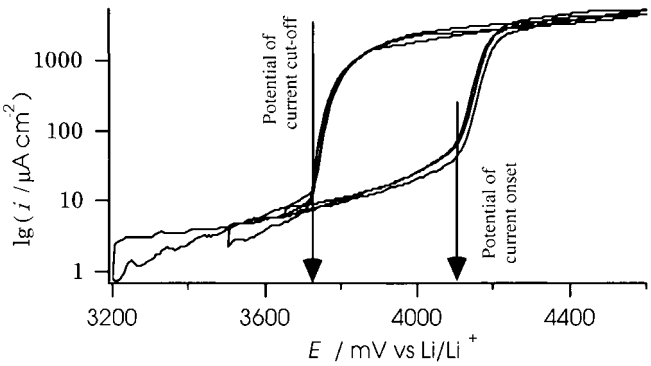

Fig. 5. Steady-state voltammetric data obtained with method 2 (semilogarithmic plot). Solutions: 1 M LiTFSI/EMC + 3% EC. Cathodic potential limits: solid line, 3.65 V; broken line, 3.50 V; dotted line, 3.20 V.

3.3. *Solution analysis*

The establishment of the corrosion product was carried out by means of an experiment with long-term electrolysis followed by solution analysis. The anode compartment contained about 2 ml of LiTFSI/EMC + 30% EC solution. 1 mA constant current was maintained for 2.5×10^4 s. The cell voltage was 4.3–4.5 V including the ohmic drop. After the electrolysis, both the anolyte and catholyte were analysed by ICP spectrometry. The surface of the lithium counterelectrode was removed by scratching and then dissolved in ethanol to perform elemental analysis.

The result of the elemental analysis is that no aluminium can be found in the catholyte or at the surface of the lithium counterelectrode (aluminium concentration was below the detection limit), therefore it is proven that the aluminium dissolved cannot either

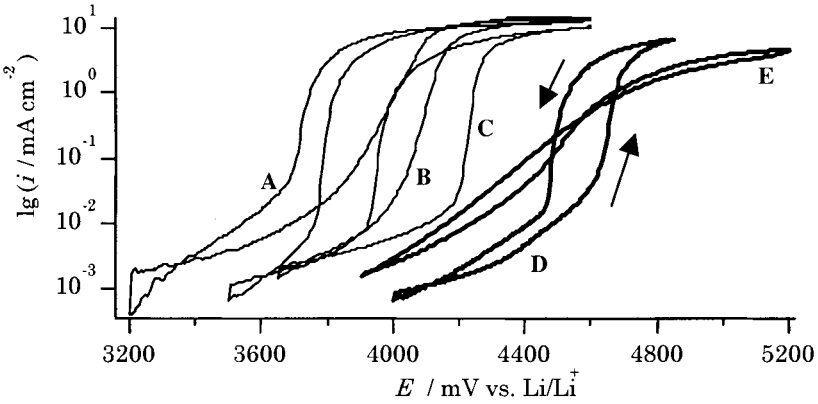

Fig. 6. Steady-state voltammetric data obtained with method 2 for the following solutions: c M LiTFSI + $(1-c)$ M LiBETI/EMC + x% EC. Concentrations: A, $c = 1$ and $x = 30$; B, $c = 0.3$ and $x = 30$; C, $c = 0.1$ and $x = 30$; D, $c = 0$ and $x = 30$; E, $c = 0$ and $x = 0$. Scan direction is indicated for curve D and the same sequence applies for the rest of the curves.

Table 2. Potentials of current onset and current cut-off of aluminium dissolution in the electrolytes studied. N/A, data not available because no linear regions suitable for extrapolation can be seen on the corresponding potentiodynamic curve

Solution composition	Potential of current onset /V vs Li	Potential of current cut-off /V vs Li
1 M LiTFSI/EMC	4.090	3.865
1 M LiTFSI/EMC + 1% EC	4.130	3.715
1 M LiTFSI/EMC + 3% EC	4.095	3.720
1 M LiTFSI/EMC + 10% EC	3.720	3.695
1 M LiTFSI/EMC + 30% EC	3.835	3.695
0.3 M LiTFSI + 0.7 M LiBETI/EMC + 30% EC	4.005	3.765
0.1 M LiTFSI + 0.9 M LiBETI/EMC + 30% EC	4.200	3.925
1 M LiBETI/EMC + 30% EC	4.615	4.470
1 M LiBETI/EMC	(N/A)	(N/A)
1 M LiTFSI/DME	4.270	3.965
1 M LiTFSI/TFPC + 50% EMC	4.235	3.840
1 M LiTFSI/TFPC	4.190	3.825
1 M LiTFSI/PC	3.550	3.550

pass the separator or deposit onto the counterelectrode. The anolyte, however, contained aluminium. The apparent charge of aluminium ions (z) was calculated with the help of Faraday's law and was obtained as $z = 3.00 \pm 0.02$ where the relative error is that of the aluminium concentration measurement. This result confirms that electrochemical dissolution of aluminium as Al^{3+} accounts for the current in the active region. Side reactions, though probably take place besides the main process, consume a negligible charge only in the potential interval of active dissolution as compared to the charge for aluminium dissolution.

3.4. *Electrochemical impedance measurements*

Impedance spectra obtained can be classified by using three categories. Spectra obtained for passive aluminium exhibit essentially the same character and therefore are discussed together. Another type of spectra was obtained for dissolving aluminium when the dissolution rate was low enough so that the mass transport did not impact substantially the dissolution kinetics. This class is named as spectra for medium-rate dissolution though the d.c. current varied in a wide range and therefore the name of the category refers to the mechanism rather then the actual reaction rate. The third sort of spectrum was observed when the influence of the mass transport on the overall dissolution kinetics was obvious from the shape of the spectra. The latter case is referred as the high-rate dissolution. This denotation also bears a mostly mechanistic meaning, similarly to the medium-rate dissolution.

Impedance spectra obtained for passive aluminium are of the same character, regardless of whether the spectra was measured with a noncorrosive system at any potential or with a corrosive system at a potential below the potential of current cut-off. The spectra are composed of one depressed semicircle with a diameter ranging from 80 kΩ cm^2 to 2 MΩ cm^2. Spectra recorded consecutively at the same potential exhibit semicircles with increasing diameter. In most of the cases, the ascending part of the arc could be measured only due to the low level of the a.c. current ($I_{ac} < 0.01$ μA for frequencies $f < 0.1$ Hz). Double layer capacitances (C_{dl}) estimated range from 3×10^{-6} to 3×10^{-5} F cm^{-2}, for electrodes covered with the native oxide close to the lower limit. No systematic dependence of the system parameters on either the solution composition or the d.c. bias potential could be established. The decay of the d.c. current took several hours during which the surface composition and the structure of the passive layer may have considerably changed.

Spectra for aluminium dissolving at a medium rate are composed of three overlapping semicircles. The semicircle occurring at the highest frequencies was always capacitive. The two other semicircles were either capacitive or inductive, depending on the solvent. In general, capacitive semicircles belong to higher frequencies than inductive semicircles if both types are detected in the same spectrum. Representative data for each type of spectrum for medium-rate aluminium dissolution are plotted in Figure 7.

Steady-state aluminium dissolution at medium rate was not available for each system investigated. Between the potentials of the current cut-off and the current onset, the d.c. current was unstable in the time scale of the impedance measurement and the spectra obtained were irreproducible which can be attributed to competitive processes like dissolution and repassivation. Nevertheless current oscillation was never detected. Aluminium dissolution at medium rate can be attained in a narrow potential interval beyond the potential of the current onset providing that the anodic current is low enough so that mass transport effects on the dissolution rate are negligible. For instance, medium-rate dissolution as defined by the character of the impedance spectra was achieved for the 1 M LiTFSI/EC + EMC systems from 0 to 10% EC content at 4.25 V but no medium-rate dissolution was observed for the 1 M LiTFSI/EMC + 30% EC solution.

Impedance spectra measured for high-rate dissolution of aluminium exhibit unusual features. First, spectra are

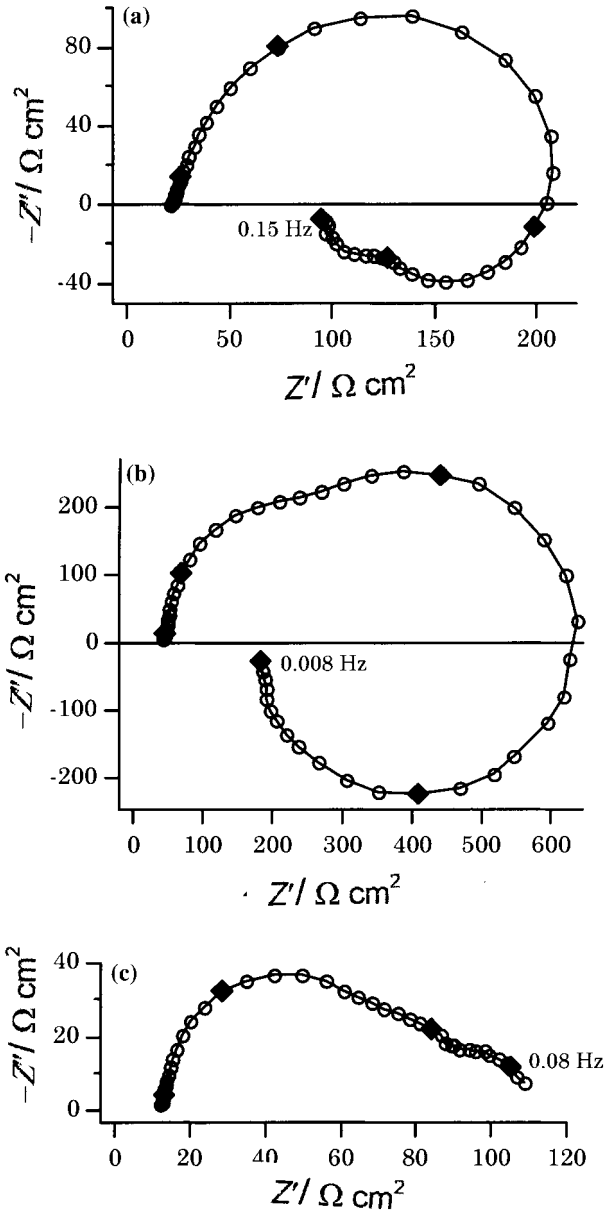

Fig. 7. Types of impedance spectra obtained for medium-rate dissolution of aluminium displayed in the Argand diagram. Solute: 1 M LiTFSI. (a) Solvent: PC + 50% EC; potential: 3.780 V. (b) Solvent: EMC + 3% EC; potential: 4.250 V. (c) Solvent: DME; potential: 4.500 V. Frequency increment between data labelled with filled diamonds, 1 decade. Lines between data are drawn as a guide to the eye.

composed of a high-frequency capacitive semicircle, a single medium-frequency inductive loop and an ascending capacitive line. The medium-frequency loop is always inductive, regardless of whether any of the semicircles is inductive in the spectra measured for medium-rate dissolution. Second, no Warburg regime can be found in the low-frequency domain. The low-frequency part of the spectra never approaches a line inclining at 45° to the real axis even at the lowest frequency measured which was usually 10 mHz. Data measured below 10 mHz are too scattered that is attributed to the occurrence of natural convection and thermal instability. A typical spectrum obtained for the 1 M LiTFSI/EMC + 30% EC system at 4.5 V is plotted in Figure 8.

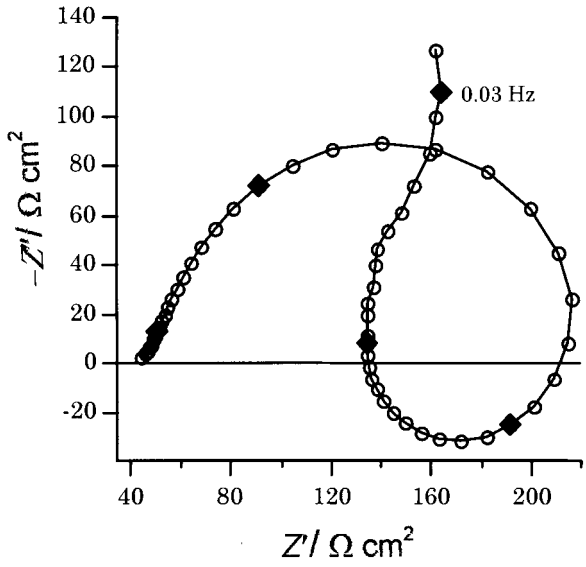

Fig. 8. Typical impedance spectrum obtained for high-rate dissolution of aluminium displayed in the Argand diagram. Solution: 1 M LiTFSI/EMC + 30% EC. Potential: 4.500 V. Frequency increment between data labelled with filled diamonds, 1 decade. Lines between data are drawn as a guide to the eye.

4. Discussion

4.1. *Passive and active states of aluminium*

The behaviour of aluminium can be characterized as follows: Aluminium is passive at the rest potential as a result of the spontaneous reduction of the solvent and the electrolyte which results in a protecting layer composed of a mixture of aluminium oxide, fluoride and carbonate [6]. $LiPF_6$ and $LiBF_4$ are excellent passivating agents because they can easily release fluoride ions which contribute to the passivation of aluminium [6]. The passive layer can protect aluminium at low anodic potentials. The protection potential strongly depends on the nature of both the solvent and the electrolyte. The increase in the relative dielectric constant of the electrolyte results in the decrease in the protection potential providing that the solvent components applied are of similar chemical structure (see alkylcarbonates such as EC and EMC). However, solvents with heteroatoms (such as TFPC) or with different functional group (such as DME) do not fit to the trend established.

LiTFSI is much more active towards aluminium dissolution than LiBETI. The potential of the current onset is independent of both the cathodic limit of the scan and the polarization sweep rate which indicates that there is no change in the properties of the passive layer and the current in the passive region corresponds to the low-rate dissolution of aluminium. However, there has to be a significant difference between the native passive layer and that produced after dissolving aluminium at a high rate. The difference in the composition and/or the compactness of the passive layers produced at different conditions may be the explanation for the

unusual discrepancy found between the responses for the polarization programs, methods 1 and 2.

EIS measurements reveal that the overall reaction takes place in several steps. The high-frequency semicircle of the impedance spectra is associated with the double layer capacitance and the charge transfer resistance while the medium-frequency and low-frequency semicircles belong to the adsorption of the intermediates. Detailed analysis of EIS measurements for both medium-rate and high-rate dissolution will be published in a forthcoming paper [15].

4.2. *Mechanism of aluminium dissolution*

The result of solution analysis after constant current dissolution indicated that the product of the reaction is Al^{3+}. EIS data show that the overall process is composed of many steps. The medium-frequency and low-frequency semicircles in the spectra obtained for medium-rate dissolution are therefore attributed to the adsorption of the intermediates which contain partially oxidized aluminium atoms, $Al^{+\bullet\bullet}$ and $Al^{++\bullet}$. It is assumed that the adsorbed intermediates are neutral and the electric neutrality is maintained by the coordination of one or two $TFSI^-$ and/or $BETI^-$. The assumption that the intermediates are insoluble is verified by the determination of z by means of solution analysis. The final composition of the product is not known; however, a few assumptions can be made. First, the number of coordinating anions around the central aluminium atom is limited by steric factors and hence two anions are taken into account. Involvement of less than two anions would also be unfavourable due to the relatively large charge of the product.

Now the reaction pattern can be written as follows:

$$Al_s + TFSI^-_{solv} \longrightarrow [Al(TFSI)]_{ads} + e^- \quad (R1)$$

$$[Al(TFSI)]_{ads} + TFSI^-_{solv} \longrightarrow [Al(TFSI)_2]_{ads} + e^- \quad (R2)$$

$$[Al(TFSI)_2]_{ads} + n\,So_{solv} \longrightarrow [Al(TFSI)_2(So)_n]^+_{solv} + e^- \quad (R3)$$

Denotation 'So' refers to the solvent. A similar reaction pattern can be assumed for $BETI^-$ with the appropriate substitution of the ligands.

The influence of the solvent, which is obvious from the data shown in the previous Sections, is considered in the desorption step only. If the solvent was involved in the stabilization of the intermediates by forming, for instance, $[Al(TFSI)(So)]_{ads}$, the number of adsorption time constants should be larger than two in case of any solvent blend because of the increase in the number of possible intermediates. However, splitting up of adsorption semicircles in the impedance spectra was never observed with solvent mixtures containing a single electrolyte. In contrast, the adsorption semicircles become distorted if the solution contains both LiTFSI and LiBETI. In the latter case, the number of intermediate does increase because two kinds of anion can be attached to the partially oxidized aluminium ion. This finding is a strong evidence for the mechanism suggested.

The mechanism described with Reactions R1–R3 gives the opportunity to elucidate the difference between the ability of $TFSI^-$ and $BETI^-$ anions towards dissolving aluminium. It is assumed that the constitution of the imide anions is intact during aluminium dissolution and they act as a complexing agent only, as shown in Reactions R1–R3. Imide anions contain a nitrogen atom with some negative charge and some nonbonding electron pairs which are suitable to be donated to the aluminium ion. We think that the nitrogen atom in the imide anion is the active centre by which the coordination takes place. This assumption is strongly supported by the fact that lithium methides with the same perfluoroalkylsulfonyl groups $[LiC(SO_2C_nF_{2n+1})_3]$ are not corrosive at all [7]. The electronic structure of the imide anions can be modelled with the possible resonance structures depicted in Figure 9. As many as nine resonance structures can be drawn that are divided into three classes. Classification is based on the charge and bonding structure of the central nitrogen atom. The structures with positive nitrogen and an S–N–S bond of theoretically 180° bonding angle in Class 3 are unusual in the sense that three atoms are charged despite localizing the single negative charge of the ion on any of the oxygen or nitrogen atoms would give a simpler resonance structure.

The S–N–S bond angle in the free-standing $TFSI^-$ anion is 115.0° (estimated from molecular orbital calculation), consequently the degree of delocalization of the nonbonding electron pairs of the nitrogen atom is low. The S–N–S bond angle of the $TFSI^-$ anion can be understood by taking into account the resonance structures in class 1 and class 2. Class 1 exhibit an approximately tetrahedral nitrogen atom with S–N–S bond angle slightly less than 109.5° due to the large steric requirement of the nonbonding pairs and class 2

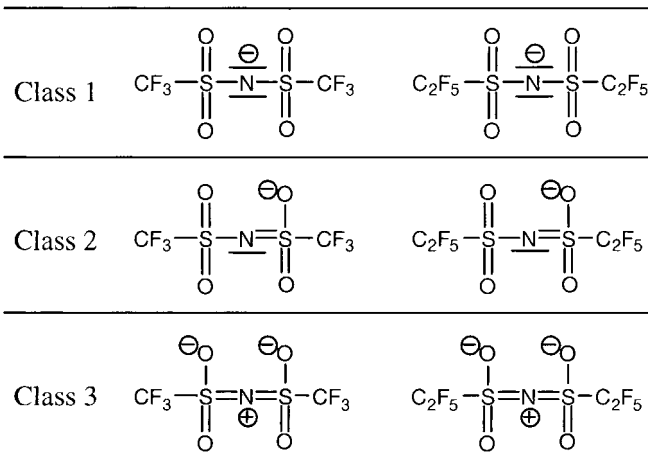

Fig. 9. Resonance structures for $TFSI^-$ and $BETI^-$ anions.

provides a bond angle very close to 120°. The value for the S–N–S bond angle obtained from the simulation is between these limiting values hence it is assumed that the structure of the $TFSI^-$ anion can be elucidated by omitting the structures in class 3.

The S–N–S bond angle in the $BETI^-$ anion is 128.3° which is larger than the typical bond angle in the structure with asymmetrically bonded nitrogen described with structures in class 2. The result of the simulation shows that the structure of the $BETI^-$ anion can be rather modelled by considering the resonance structures of classes 2 and 3. The large S–N–S bond angle means that the delocalization of the electron pairs is more complete in the $BETI^-$ anion than in the $TFSI^-$ anion. This is in excellent agreement with the assumption that the perfluoroethyl groups have larger electron withdrawing power than perfluoromethyl groups. Additionally, the enlarged repulsion of the larger perfluoroalkyl groups stretches the ion along the S–N–S axis, resulting in larger S–N–S bond angle. Therefore the complexing ability of the $BETI^-$ anion is reduced as compared to the $TFSI^-$ anion.

The free energy of the intermediates can be diminished considerably by a strongly complexing anion. The potential difference observed in the aluminium dissolution in the presence of $BETI^-$ and $TFSI^-$ can be perfectly explained with the molecular structure of the anions and the stability of their complex with aluminium ion.

The variation in the current in the transpassive region can also be elucidated by considering the properties of the solvents and the products. In case of EMC + EC blends, the current in the regime of active dissolution increases with the concentration of EC. EC can accelerate the electrochemical desorption of the complex (Reaction R3) due to its relatively large dipole moment and hence it is capable of stabilizing the product. The ability of EC (or PC) to solvate the complex and stabilize the product offsets the impact of the decreased diffusivity of $TFSI^-$ in the mixtures of large EC content with higher viscosity. In case of the $BETI^-$ anion, however, the potential interval of the active dissolution does not depend significantly on the concentration of the large dipole moment cosolvent (Figure 7). It is assumed that the stabilization effect is negligible in case of $BETI^-$ due to the bigger size of the aluminium–BETI complex and probably also by the smaller number of strongly coordinating solvent molecules in the first solvation shell.

4.3. *Application of LiBPSIs in batteries*

Our results show that aluminium, which is almost exclusively used as cathode current collector in rechargeable lithium ion batteries, is not compatible with LiTFSI. Even if the potential of current onset is beyond the theoretical anodic potential limit of the charging half cycle, overcharge leads to the activation of aluminium. Since repassivation with most of the solutions takes place at a potential well within the normal operation potential interval of high-voltage cathodes, self-discharge of the cathode may substantially reduce the cell capacity. Furthermore, dissolved aluminium can be redeposited at the negative electrode and thus modify its charge-discharge characteristics. In thin layer batteries redeposition of aluminium is a possible process, in contrast of our cell used for bulk electrolysis, since the distance of aluminium ion diffusion is only a few tens of micrometres. The cell will be ultimately destroyed by the loss of mechanical integrity of the anode as a result of the large amount of dissolved aluminium. Aluminium deposition to the anode also blocks the lithium ion flow from and to the carbonaceous material that is detrimental for cell operation. Therefore, either aluminium current collectors should be replaced with a noncorroding metal or less corrosive salts should be employed. According to our results, LiBETI can be appropriate if the solvent is carefully selected.

Correlation of the structure of the imide anions and their inclination to promote aluminium dissolution is very important because it yields an opportunity to design new noncorrosive lithium imides for battery application. It can be anticipated from our results that imides with large S–N–S bond angle and hence with no ability of electron pair donation can be the most successful candidates in lithium ion battery application in the sense of the current collector protection. These structural features are probably achievable by means of either adding bulky terminal groups whose steric effects determines the structure of the imide anion or fixing the nitrogen atom in a ring which does not allow the S–N–S bond angle to decrease.

References

1. D.H. Jang and S.M. Oh, *J. Electrochem. Soc.* **144** (1997) 3342.
2. Y. Xia, Y. Zhou and M. Yoshio, *J. Electrochem. Soc.* **144** (1997) 2593.
3. G.G. Amatucci, J.M. Tarascon and L.C. Klein, *Solid State Ionics* **83** (1996) 167.
4. J. Barthel, R. Buestrich, H.J. Gores, M. Schmidt and M. Wühr, *J. Electrochem. Soc.* **144** (1997) 3866.
5. A. Webber, *J. Electrochem. Soc.* **138** (1991) 2586.
6. L.J. Krause, W. Lamanna, J. Summerfield, M. Engle, G. Korba, R. Loch and R. Atanasoski, *J. Power Sources* **68** (1997) 320.
7. C.A. Vincent and B. Scrosati, 1997. *Modern Batteries* 2nd edn, Arnold, p. 219.
8. M. Winter and P. Novák, *J. Electrochem. Soc.* **145** (1998) L27.
9. Y. Ein-Eli, S.R. Thomas, R. Chadha, T.J. Blakley and V.R. Koch, *J. Electrochem. Soc.* **144** (1997) 823.
10. D. Aurbach, Y. Ein-Eli, B. Markovsky, A. Zaban, S. Luski, Y. Carmeli and H. Yamin, *J. Electrochem. Soc.* **142** (1995) 2882.
11. Y. Ein-Eli, S.R. Thomas, V.R. Koch, D. Aurbach, A. Schechter and B. Markovsky, *J. Electrochem. Soc.* **143** (1996) L273.
12. Y. Ein-Eli, S.F. McDevitt, D. Aurbach, B. Markovsky and A. Schechter, *J. Electrochem. Soc.* **144** (1997) L180.
13. J. Braithwaite, G. Nagasubramanian, A. Gonzales, S. Lucero and W. Cieslak, *The Electrochemical Society Proceedings Series*, **PV 96-17**, Pennington, NJ, (1996) p. 44.
14. J.B. Foresman and A. Frisch, *Exploring Chemistry with Electronic Structure Methods*, 2nd edn, Gaussian, Inc., Pittsburg, PA.
15. L. Péter, J. Arai and H. Akahoshi, in preparation.